Accurate pHEMT Nonlinear Modeling in the Presence of Low-Frequency Dispersive Effects

Antonio Raffo, *Student Member, IEEE*, Alberto Santarelli, *Member, IEEE*, Pier Andrea Traverso, *Member, IEEE*, Giorgio Vannini, *Member, IEEE*, Francesco Palomba, Francesco Scappaviva, Maurizio Pagani, and Fabio Filicori

***Abstract*—Low-frequency (LF) dispersive phenomena due to device self-heating and/or the presence of "traps" (i.e., surface state densities and bulk spurious energy levels) must be taken into account in the large-signal dynamic modeling of III–V field-effect transistors when accurate performance predictions are pursued, since these effects cause important deviations between direct current (dc) and dynamic drain current characteristics. In this paper, a new model for the accurate characterization of these phenomena above their cutoff frequencies is presented, which is able to fully exploit, in the identification phase, large-signal current–voltage (I–V) measurements carried out under quasi-sinusoidal regime using a recently proposed setup. Detailed experimental results for model validation under LF small- and large-signal operating conditions are provided. Furthermore, the I–V model proposed has been embedded into a microwave large-signal pseudomorphic high electron-mobility transistor (pHEMT) model in order to point out the strong influence of LF modeling on the degree of accuracy achievable under millimeter-wave nonlinear operation. Large-signal experimental validation at microwave frequencies is provided for the model proposed, by showing the excellent intermodulation distortion (IMD) predictions obtained with different loads despite the very low power level of IMD products involved. Details on the millimeter-wave IMD measurement setup are also provided. Finally, IMD measurements and simulations on a Ka-band highly linear power amplifier, designed by Ericsson using the Triquint GaAs 0.25-μm pHEMT process, are shown for further model validation.**

***Index Terms*—Field-effect transistors (FETs), intermodulation distortion (IMD), nonlinear circuits, nonlinear distortion, semiconductor device modeling.**

I. Introduction

LARGE-SIGNAL modeling of low-frequency (LF) dispersive phenomena in electron devices strongly influences the capability of obtaining accurate performance predictions also at microwave and millimeter-wave frequencies, especially when nonlinear operation is involved [1]–[4]. This issue, sometimes ignored in the past years, has proved as extremely important in the context of empirical modeling of electron devices for monolithic microwave integrated circuit (MMIC) design. Unfortunately, large-signal modeling of the LF[1] dynamic behavior of electron devices cannot be simply based on static current–voltage (I–V) characteristics, when accurate predictions are required. In fact, thermal effects (such as device self-heating and/or case temperature variations) and the presence of deep level traps and surface state densities in III–V field-effect transistors (FETs) cause important deviations between static and LF dynamic drain current characteristics.

Many efforts have been made by several research groups to take into account LF dispersion in both lookup-table-based and equivalent circuit models [4]–[14]. In this paper, an accurate empirical large-signal model is proposed, for the prediction of the device drain I–V behavior, under dynamic operation above the cutoff frequencies of dispersive phenomena. The approach, which is based on the definition of a small set of purely algebraic model functions to be characterized by evaluating the associated lookup tables within the regions of interest, is inherently independent of the device technology. The hypotheses involved in the analytical development of the model, which assume the operation of the device as being mildly nonlinear with respect to state variables describing the dispersive phenomena, when compared to the main nonlinearities in the FET behavior (such as the channel modulation), lead to reasonable approximations, which are quite commonly adopted in the literature and robustly verified by experimental evidence.

The identification of the model functions can be carried out through conventional dc I–V measurements at different case temperatures and small-signal (SS) bias-dependent ac measurements at LFs. In addition, the extraction of the proposed model could be made more robust and the prediction performance more accurate by means of pulsed I–V measurements, especially when nonlinear operation is involved. Indeed, pulsed measurements are largely adopted by many modeling approaches as they allow for a more exhaustive large-signal characterization above the cutoff of device dispersion [14]–[18]. Nevertheless, pulsed I–V systems represent

Manuscript received April 7, 2005; revised July 31, 2005. This work was supported in part by the Italian Ministry of Instruction, University and Research and also performed in the context of the network Top Amplifier Research Groups in a European Team supported by the Information Society Technologies Programme of the European Union under Contract IST-1-507893-NOE.

A. Raffo is with the Department of Engineering, University of Ferrara, Ferrara 44100, Italy and also with CoRiTeL, Morena, Rome 00040, Italy (e-mail: araffo@ing.unife.it).

A. Santarelli, P. A. Traverso, and F. Filicori are with the Department of Electronics, University of Bologna, Bologna 40136, Italy (e-mail: asantarelli@deis.unibo.it; ptraverso@deis.unibo.it; ffilicori@deis.unibo.it).

G. Vannini is with the Department of Engineering, University of Ferrara, Ferrara 44100, Italy (e-mail: gvannini@ing.unife.it).

F. Palomba and M. Pagani are with Ericsson Laboratory Italy S.p.A., Vimodrone (MI) 20090, Italy (e-mail: francesco.palomba@ericsson.com; maurizio.pagani@ericsson.com).

F. Scappaviva is with Microwave Electronics for Communications S.r.l. (MEC), Bologna 40123, Italy (e-mail: francesco.scappaviva@mec-mmic.com).

Digital Object Identifier 10.1109/TMTT.2005.859034

[1]Although the trapping and thermal dispersion in electron devices takes place typically between a few hertz and some hundreds of kilohertz, the present modeling approach deals with "above-dispersion-cutoff" operation. For this reason, the LF term is used in the paper with reference to a range between the upper frequencies of dispersive phenomena (e.g., 1 MHz) and the lowest frequency, at which reactive effects related to charge storage variations and finite transit times cannot be further neglected (e.g., 1 GHz).

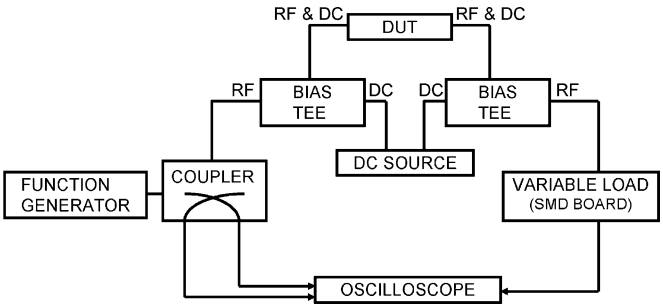

Fig. 1. Recently proposed large-signal measurement setup. From [19].

rather sophisticated setups, which provide reliable results only when suitably operated, and are not always available in microwave laboratories. For these reasons, an alternative large-signal I–V measurement system has been recently presented [19], where the device-under-test (DUT) is excited simply by an LF large-signal sinusoidal voltage source as shown in Fig. 1; such a setup can be easily implemented by means of conventional commercial instrumentation. In the present work, the proposed large-signal acquisition system is exploited in order to characterize the LF dispersion in I–V characteristics of a III–V FET.

This paper is organized as follows. The analytical development of the new empirical I–V model is discussed in details in Section II, along with the experimental steps needed for the characterization of model functions. Two slightly different formulations are proposed, according to the degree of accuracy pursued in the description of above-cutoff thermal dispersion, while the discussion on the extraction procedure points out how different experimental large-signal techniques can be exploited. In Section III, the LF I–V model is identified for a 0.25-μm Triquint GaAs pseudomorphic high electron-mobility transistor (pHEMT) ($W = 600$ μm) and is then embedded into a large-signal device model for microwave and millimeter-wave applications (namely, the nonlinear discrete convolution (NDC) model [2]), and the experimental validation at both LFs (2 MHz) and high frequencies (microwaves) is presented. Finally, intermodulation distortion (IMD) predictions of a pHEMT-based highly linear power amplifier (PA) at Ka-band, designed and realized by Ericsson Laboratory Italy, are shown. Details about the intermodulation measurement system adopted and its calibration procedure are provided as well.

II. LF I–V Modeling in III–V FETs

A. Formulation of the "Above-Cutoff" Dispersion Model

In microwave circuit harmonic balance (HB) analysis, the lowest RF spectral component to be considered is usually well above the cutoff frequencies associated with dispersive phenomena. Under such condition, any possible set of state variables $\underline{x}(t)$, which can be chosen in order to describe the "slow" dynamic phenomena associated with traps, is practically coincident with its time-averaged mean value $\underline{X}_0$. Similar considerations are valid for the channel temperature, that is, $\vartheta(t) \cong \vartheta_0$. As a common choice in the context of circuit design-oriented device modeling, the temperature is also assumed as being uniform along the channel. Thus, at frequencies above the cutoff of dispersive phenomena, but low enough to neglect the microwave reactive effects due to charge storage variations and/or finite transit times, the drain current of a III–V FET can be expressed as

$$i_d(t) = \Psi\left[v_g(t), v_d(t), \underline{X}_0, \vartheta_0\right] \tag{1}$$

where Ψ is a purely algebraic nonlinear function, while $v_g(t)$ and $v_d(t)$ are the instantaneous values of the voltages (referred to the source terminal) applied at the device ports.

The vector $\underline{X}_0$ of the dc components of the state variables associated with traps is here assumed as being dependent only on the mean values V_{g0}, V_{d0} of the external voltages $v_g(t)$ and $v_d(t)$. In fact, both experimental evidence and simulation results confirm that the device trapping state $\underline{X}_0$ is not significantly affected by any "direct" ac-to-dc conversion,[2] i.e., the ac components above dispersion cutoff of the voltages at device ports do not influence in a significant way the distribution of carriers within trapping spurious energy levels. Moreover, the well-known and largely adopted pulsed I–V techniques [14]–[18] are based on the assumption that the state $\underline{X}_0$, which is associated with the device quiescent point (V_{g0}, V_{d0}) before the application of the superimposed voltage pulses, is not perturbed by either the pulse "shape" or amplitudes (i.e., by second and higher moments of the pulse waveforms) during the measurement of the device currents. Thus, (1) can be replaced by

$$i_d(t) \cong F\left[v_g(t), v_d(t), V_{g0}, V_{d0}, \vartheta_0\right]. \tag{2}$$

According to conventional approaches, ϑ_0 will be considered in the following as being linearly dependent on the average dissipated power under dynamic conditions P_0, i.e.,

$$\vartheta_0 = \vartheta_c + R_\vartheta P_0 \tag{3}$$

where ϑ_c is the case (or substrate) temperature and R_ϑ is the device thermal resistance.

The dependence of the drain current LF model on (V_{g0}, V_{d0}, ϑ_0) has been indicated in (2) as being as general as possible. Nevertheless, mild simplifying hypotheses can be introduced in order to identify a practically useful model formulation, which preserves an adequate degree of predictive accuracy and, at the same time, can be characterized by means of reliable experimental procedures and easily implemented for MMIC analysis and design. More precisely, the effects of dispersive phenomena on the dynamic drain current when only above-cutoff frequencies are involved in the device operation can be considered as being mildly nonlinear, or practically linear. Such an approximation, which has been successfully verified and adopted in the past [21], [23], can be further justified by noting that trapping phenomena in FETs are physically distributed either along surface contact regions, or inside the bulk structure, i.e., they exert their influence in regions, which are "peripheral" and well distinct from the channel, whose conductance modulation due to

[2]An indirect ac-to-dc conversion between $\underline{x}(t) \approx \underline{X}_0$ and $v_g(t)$, $v_d(t)$ is, however, possible, in the sense that, under large-signal operation, the time-averaged mean values V_{g0}, V_{d0}, on which the trapping state is supposed to depend, can be different from the corresponding bias values due to device nonlinearity and bias-tee nonidealities. Such a conversion is taken into account in the model through the dependence on V_{g0}, V_{d0}, which will be introduced later in this paper.

$v_g(t)$, $v_d(t)$ represents instead the main nonlinear phenomenon affecting the device behavior. Moreover, if higher order terms in the Taylor series expansion of (2) with respect to (V_{g0}, V_{d0}) were needed even for an acceptably approximated description of the above-cutoff dispersion, this would be somehow in contrast with the well-verified above-discussed assumption of neglecting the dependence of the dynamic drain current (2) on second and higher moments of $v_g(t)$, $v_d(t)$ (e.g., root mean square (rms) values). Thus, the linearization of (2) with respect to V_{g0}, V_{d0}, P_0, ϑ_c around a generic V_{g0}^*, V_{d0}^*, P_0^*, ϑ_c^* condition leads, after some algebraic manipulations, to the drain current LF model formulation [21] given as

$$\begin{aligned} i_d(t) = & F_{\rm DC}^*\left[v_g(t), v_d(t)\right] \\ & + f_\vartheta\left[v_g(t), v_d(t)\right]\left(R_\vartheta\left(P_0^* - P_0\right) + \vartheta_c^* - \vartheta_c\right) \\ & + f_g\left[v_g(t), v_d(t)\right]\left(v_g(t) - V_{g0}\right) \\ & + f_d\left[v_g(t), v_d(t)\right]\left(v_d(t) - V_{d0}\right) \end{aligned} \tag{4}$$

where the model functions $F_{\rm DC}^*$, f_g, f_d, and f_ϑ can be easily related to the $F(\cdot)$ function by the following relationships:

$$\begin{aligned} f_g &= -\left.\frac{\partial F}{\partial V_{g0}}\right|_* \\ f_d &= -\left.\frac{\partial F}{\partial V_{d0}}\right|_* \\ f_\vartheta &= -\left.\frac{\partial F}{\partial \vartheta_0}\right|_* \end{aligned} \tag{5a}$$

$$\begin{aligned} F_{\rm DC}^* = & \left.F\left[v_g(t), v_d(t), V_{g0}, V_{d0}, \vartheta_0\right]\right|_* \\ & + f_g\left[v_g(t), v_d(t)\right]\left(V_{g0}^* - v_g\right) \\ & + f_d\left[v_g(t), v_d(t)\right]\left(V_{d0}^* - v_d\right). \end{aligned} \tag{5b}$$

These four model functions are purely algebraic nonlinear relationships with respect to the instantaneous values of the voltages applied to the device ports. They can be described within the regions of interest through suitable lookup tables, as shown in Section II-C. Since the linearization of (2) has been carried out with respect to (V_{g0}, V_{d0}, ϑ_0) only, no approximation is introduced on the dependence of $F_{\rm DC}^*$, f_g, f_d, and f_ϑ with respect to the large-signal voltages at the device ports.

The functions f_g and f_d in (5) describe the deviations between the static and the dynamic drain current response due to traps above their cutoff, while f_ϑ accounts for deviations caused by variations in power dissipation and/or case temperature θ_c. The term $F_{\rm DC}^*$, instead, represents the equithermal dc drain current characteristic or the dc characteristic ideally "measured" at the constant channel temperature ϑ_0^*. Evidently, the term $F_{\rm DC}^*$ cannot be directly related to any measured characteristics. In order to avoid the presence of such a term, a modified formulation for the thermal model is adopted in the following. To this end, it is convenient to define an instantaneous power $p_s(t)$ as

$$p_s(t) = v_d(t) F_{\rm DC}\left[v_g(t), v_d(t), \vartheta_c\right] \tag{6}$$

which represents a "quasi-static" term corresponding to the power that would be dissipated if $v_g(t)$ and $v_d(t)$ were "slowly" time-varying voltages [20], with $F^{\rm DC}[v_g(t), v_d(t), \vartheta_c]$ being

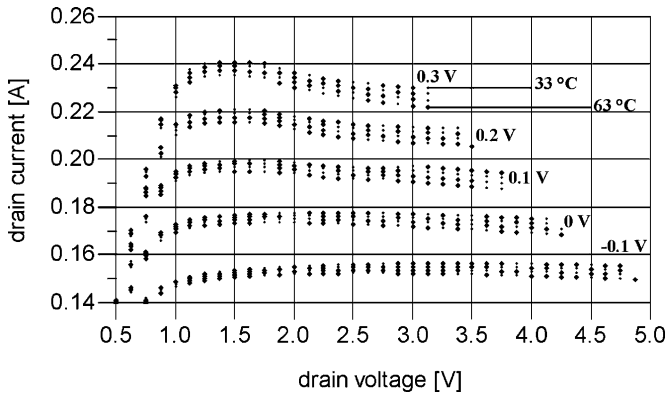

Fig. 2. Static drain current measurements carried out at different case temperatures with V_{g0} $[-0.1; 0.3]$.

the static drain current at a constant case temperature ϑ_c. Thus, (4) can be rewritten as

$$\begin{aligned} i_d(t) = & F_{\rm DC}^*\left[v_g(t), v_d(t)\right] \\ & + f_\vartheta\left[v_g(t), v_d(t)\right]\left(R_\vartheta\left(P_0^* - p_s(t)\right) + \vartheta_c^* - \vartheta_c\right) \\ & + f_\vartheta\left[v_g(t), v_d(t)\right]\left(R_\vartheta\left(p_s(t) - P_0\right)\right) \\ & + f_g\left[v_g(t), v_d(t)\right]\left(v_g(t) - V_{g0}\right) \\ & + f_d\left[v_g(t), v_d(t)\right]\left(v_d(t) - V_{d0}\right) \end{aligned} \tag{7}$$

where the term $p_s(t)$ has simply been added and subtracted.

Under static conditions, the quasi-static power $p_s(t)$ coincides with P_0 and the dynamic voltage values coincide with their average values V_{g0}, V_{d0}, so that for a generic case temperature θ_c, it holds that

$$\begin{aligned} I_{d0} = & F_{\rm DC}^*[V_{g0}, V_{d0}] + f_\vartheta[V_{g0}, V_{d0}] \\ & \times \left(R_\vartheta\left(P_0^* - p_s(t)\right) + \vartheta_c^* - \vartheta_c\right) \\ = & F_{\rm DC}[V_{g0}, V_{d0}, \vartheta_c] \end{aligned} \tag{8}$$

which evidently represents the nonequithermal static drain current characteristic at a constant case temperature ϑ_c. The term $F_{\rm DC}[V_{g0}, V_{d0}, \vartheta_c]$ can be linearized with respect to the case temperature ϑ_c

$$\begin{aligned} F_{\rm DC}[V_{g0}, V_{d0}, \vartheta_c] \cong & F_{\rm DC}\left[V_{g0}, V_{d0}, \vartheta_c^*\right] \\ & + f_{\vartheta_c}[V_{g0}, V_{d0}]\left(\vartheta_c^* - \vartheta_c\right) \end{aligned} \tag{9}$$

where

$$f_{\vartheta_c} = -\left.\frac{\partial F_{\rm DC}\left(v_g(t), v_d(t), \vartheta_c\right)}{\partial \vartheta_c}\right|_*. \tag{10}$$

Such an approximation is reasonable due to the small deviations of the drain current with respect to case temperature variations as can be seen in Fig. 2.

From (7)–(10), under dynamic conditions and above the cutoff of dispersive phenomena, a new model formulation is obtained as follows:

$$\begin{aligned} i_d(t) = & F_{\rm DC}\left[v_g(t), v_d(t), \vartheta_c^*\right] + f_{\vartheta_c}\left[v_g(t), v_d(t)\right]\left(\vartheta_c^* - \vartheta_c\right) \\ & + f_\vartheta\left[v_g(t), v_d(t)\right]\left(R_\vartheta\left(p_s(t) - P_0\right)\right) \\ & + f_g\left[v_g(t), v_d(t)\right]\left(v_g(t) - V_{g0}\right) \\ & + f_d\left[v_g(t), v_d(t)\right]\left(v_d(t) - V_{d0}\right). \end{aligned} \tag{11}$$

In this expression, the functions f_ϑ and f_{ϑ_c} account, respectively, for the dynamic current deviations, with respect to the actual dc characteristic at the case temperature ϑ_c^*, due to thermal effects such as self-heating and/or case temperature variations.

B. Link Between f_ϑ and f_{ϑ_c}

The two functions used for the characterization of the thermal behavior of electron devices f_ϑ and f_{ϑ_c} can be related by means of simple considerations. Under static conditions, (2) and (11) must be obviously coincident as follows:

$$F[V_{g0}, V_{d0}, V_{g0}, V_{d0}, \vartheta_0] = F_{\rm DC}[V_{g0}, V_{d0}, \vartheta_c] \tag{12}$$

where $\vartheta_0 = \vartheta_c + R_\vartheta P_0$ and

$$P_0 = V_{d0} F_{\rm DC}[V_{g0}, V_{d0}, \vartheta_c]. \tag{13}$$

From (12), we have

$$\begin{aligned} f_{\vartheta_c}[V_{g0}, V_{d0}] &= -\left.\frac{\partial F_{\rm DC}(V_{g0}, V_{d0}, \vartheta_c)}{\partial \vartheta_c}\right|_* \\ &= -\left.\frac{\partial F(V_{g0}, V_{d0}, V_{g0}, V_{d0}, \vartheta_0)}{\partial \vartheta_c}\right|_* \\ &= -\left.\frac{\partial F(V_{g0}, V_{d0}, V_{g0}, V_{d0}, \vartheta_0)}{\partial \vartheta_0}\right|_* \left.\frac{\partial \vartheta_0}{\partial \vartheta_c}\right|_* \\ &= f_\vartheta[V_{g0}, V_{d0}] \left.\frac{\partial \vartheta_0}{\partial \vartheta_c}\right|_* \end{aligned} \tag{14}$$

where (5) has been taken into account. Moreover, from (3),

$$\begin{aligned} \left.\frac{\partial \vartheta_0}{\partial \vartheta_c}\right|_* &= 1 + R_\vartheta V_{d0} \left.\frac{\partial F_{\rm DC}[V_{g0}, V_{d0}, \vartheta_c]}{\partial \vartheta_c}\right|_* \\ &= 1 - R_\vartheta V_{d0} f_{\vartheta_c}[V_{g0}, V_{d0}]. \end{aligned} \tag{15}$$

By substituting (15) in (14), the following relationship between the two functions f_ϑ and f_{ϑ_c} is found:

$$\begin{aligned} &f_{\vartheta_c}[V_{g0}, V_{d0}] \\ &\quad = f_\vartheta[V_{g0}, V_{d0}] \left.\frac{\partial \vartheta_0}{\partial \vartheta_c}\right|_* \\ &\quad = f_\vartheta[V_{g0}, V_{d0}] \left(1 - R_\vartheta V_{d0} f_{\vartheta_c}[V_{g0}, V_{d0}]\right) \end{aligned} \tag{16}$$

or, equivalently,

$$f_\vartheta[V_{g0}, V_{d0}] = \frac{f_{\vartheta_c}[V_{g0}, V_{d0}]}{1 - R_\vartheta V_{d0} f_{\vartheta_c}[V_{g0}, V_{d0}]}. \tag{17}$$

Apart from reducing the number of unknown functions to be identified, (17) allows for a simplification of the model (11), when it is possible to consider f_ϑ and f_{ϑ_c} almost coincident, as will be discussed in the next section. In this case, (11) becomes

$$\begin{aligned} i_d(t) = &F_{\rm DC}\left[v_g(t), v_d(t), \vartheta_c^*\right] \\ &+ f_{\vartheta_c}\left[v_g(t), v_d(t)\right]\left(\vartheta_c^* - \vartheta_c + R_\vartheta\left(p_s(t) - P_0\right)\right) \\ &+ f_g\left[v_g(t), v_d(t)\right]\left(v_g(t) - V_{g0}\right) \\ &+ f_d\left[v_g(t), v_d(t)\right]\left(v_d(t) - V_{d0}\right). \end{aligned} \tag{18}$$

C. Model Identification Procedure

In order to identify the model, (11) can be initially evaluated under static operating conditions. This enables, by means of static measurements at different case temperatures, the identification of the unknown function f_{ϑ_c} as

$$f_{\vartheta_c}[V_{g0}, V_{d0}] = \frac{F_{\rm DC}^{\rm meas}[V_{g0}, V_{d0}, \vartheta_c] - F_{\rm DC}^{\rm meas}[V_{g0}, V_{d0}, \vartheta_c^*]}{(\vartheta_c^* - \vartheta_c)} \tag{19}$$

where $F_{\rm DC}^{\rm meas}[V_{g0}, V_{d0}, \vartheta_c^*]$ and $F_{\rm DC}^{\rm meas}[V_{g0}, V_{d0}, \vartheta_c]$ are the measured drain current characteristics at the reference case temperature ϑ_c^* and at a different case temperature ϑ_c, respectively. In order to make the model identification more robust, model function (19) could be evaluated at different case temperatures ϑ_c, choosing the average value assumed by the function f_{ϑ_c} for each (V_{g0}, V_{d0}). During this step, it is also possible to evaluate (17) in order to verify if the simplified model formulation (18) can be adopted instead of (11).

The remaining unknown model functions f_g and f_d are then identified by minimizing the squared deviations between model predictions based on (11) and the corresponding dynamic measurements obtained under different operating conditions. To this end, the extraction procedure can be based either on the fitting of LF (e.g., 1 MHz) SS ac measurements only, or, in a more robust way when nonlinear operation is involved, also of large-signal data obtained under pulsed or quasi-sinusoidal [19] LF operation. In any case, due to the linear dependence of parameters in model formulation, the identification procedure can be carried out in closed form, avoiding nonlinear numerical optimization techniques. Such procedure will be adopted in the next section.

A summary of the main experimental and numerical successive steps involved in the extraction of the LF I–V dispersive model is shown in Fig. 3.

III. Experimental Results

A. Model Extraction

The new model formulation was identified for a 0.25-μm Triquint GaAs pHEMT ($W = 600$ μm) with the aim of obtaining an LF model suitable for very accurate predictions when embedded into a nonlinear microwave model at millimeter frequencies. In particular, the model was tested in the design of highly linear PAs, oriented to point-to-point and point-to-multipoint high-capacity radio links. Following the outlined identification procedure, static drain current measurements were carried out at different case temperatures. In particular, 33 °C was arbitrarily chosen as the reference case temperature ϑ_c^* while measurements were also performed at 43, 53, and 63 °C. The static drain characteristics in the high-dissipation region, where the self-heating effect is more important, are shown in Fig. 2.

Exploiting these measurements, f_{ϑ_c} was identified according to (19), then (17) was adopted to evaluate the possibility of using the simplified model formulation (18) instead of (11). As expected, the two functions f_ϑ and f_{ϑ_c} were found very similar one to each other except for slight deviations in the highest

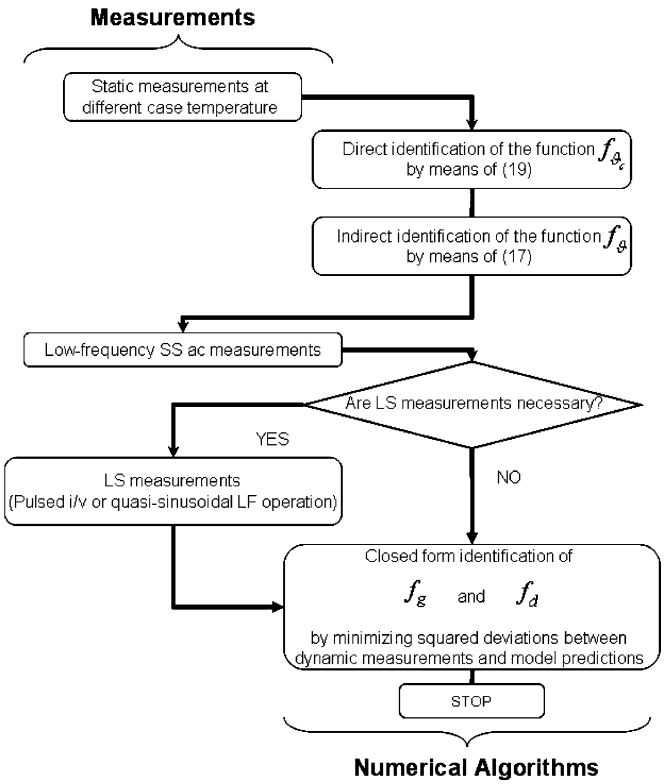

Fig. 3. Model function extraction procedure flowchart.

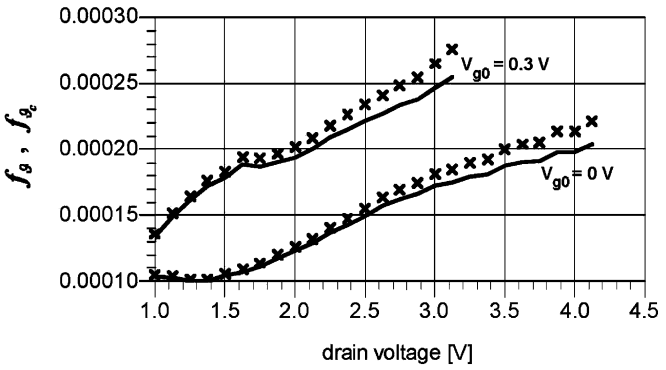

Fig. 4. Comparison between the two functions f_ϑ (crosses) and f_{ϑ_c} (solid lines) for $V_{g0} = 0$ V and $V_{g0} = 0.3$ V.

power dissipation region (highest values of the couple V_{g0}, V_{d0}), as shown in Fig. 4.

Due to the choice of the quiescent condition (class-A like) and the limited signal amplitude involved, the two functions f_ϑ and f_{ϑ_c} are here considered almost coincident. In fact, the high-power-dissipation regions are scarcely involved in the dynamic operation of highly linear PAs. Thus, model (18) was adopted as the most suitable for our application. Finally, a constant case temperature operation is also considered here: $\vartheta_c = \vartheta_c^*$.

Under these hypotheses, differentiation of (18) with respect to $v_g(t)$ and $v_d(t)$ around a generic bias condition (V_{g0}, V_{d0}) leads to

$$g_m^{\rm ac}[V_{g0}, V_{d0}] = g_m^{\rm DC}[V_{g0}, V_{d0}] + f_g[V_{g0}, V_{d0}] + f_{\vartheta_c}[V_{g0}, V_{d0}] R_\vartheta g_m^{\rm DC}[V_{g0}, V_{d0}] V_{d0} \quad (20)$$

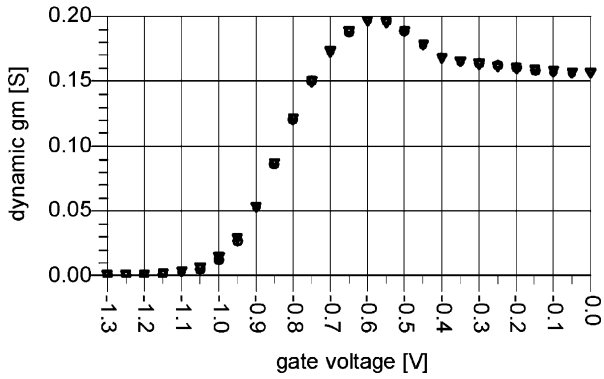

Fig. 5. Transconductance of a 0.25-μm Triquint GaAs pHEMT at different gate bias conditions and $V_{d0} = 5$ V ($f = 2$ MHz). Measurements (circles) versus predictions based on the model presented (triangles).

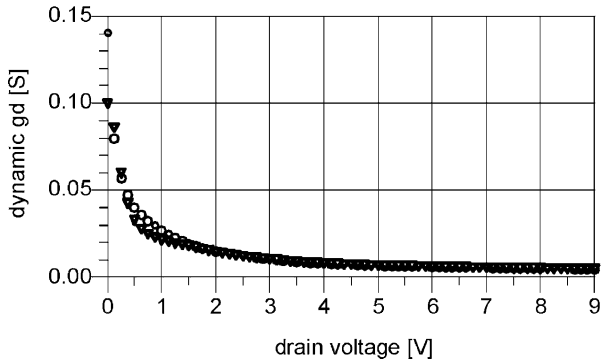

Fig. 6. Output conductance of a 0.25-μm Triquint GaAs pHEMT at different drain bias conditions and $V_{g0} = -0.5$ V ($f = 2$ MHz). Measurements (circles) versus predictions based on the model presented (triangles).

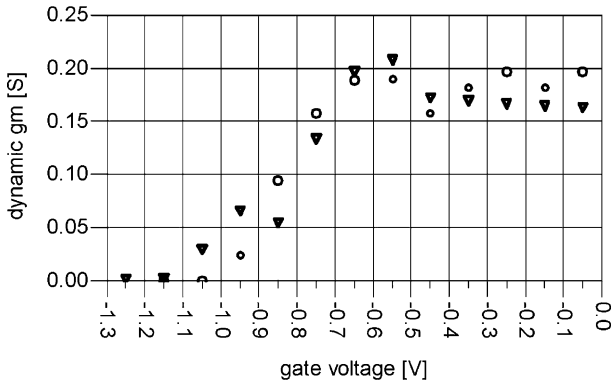

Fig. 7. Pulsed transconductance of a 0.25-μm Triquint GaAs pHEMT at different gate voltage values and $v_d = 5$ V (bias : $V_{g0} = -0.5$ V and $V_{d0} = 5$ V). Measurements (circles) versus predictions based on the model presented (triangles).

$$g_d^{\rm ac}[V_{g0}, V_{d0}] = g_d^{\rm DC}[V_{g0}, V_{d0}] + f_d[V_{g0}, V_{d0}] + f_{\vartheta_c}[V_{g0}, V_{d0}] \times R_\vartheta \left(g_d^{\rm DC}[V_{g0}, V_{d0}] V_{d0} + I_{d0} \right) \quad (21)$$

where $g_m^{\rm ac}$, $g_d^{\rm ac}$, $g_m^{\rm DC}$, and $g_d^{\rm DC}$ represent the transconductance and output conductance under LF (ac) and static (dc) conditions, while I_{d0} is the static drain current. A known value $R_\vartheta = 95$ °C/W was assumed here for the thermal resistance.

For each (v_g, v_d) pair, the two model functions f_g and f_d, are identified by minimizing the squared discrepancies between

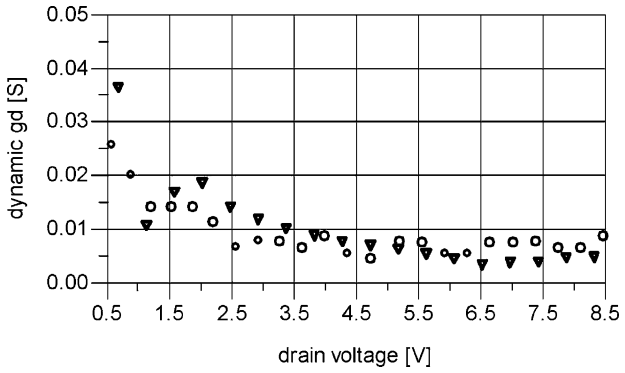

Fig. 8. Pulsed output conductance of a 0.25-μm Triquint GaAs pHEMT at different drain voltage values and $v_g = -0.5$ V (bias : $V_{g0} = -0.5$ V and $V_{d0} = 5$ V). Measurements (circles) versus predictions based on the model presented (triangles).

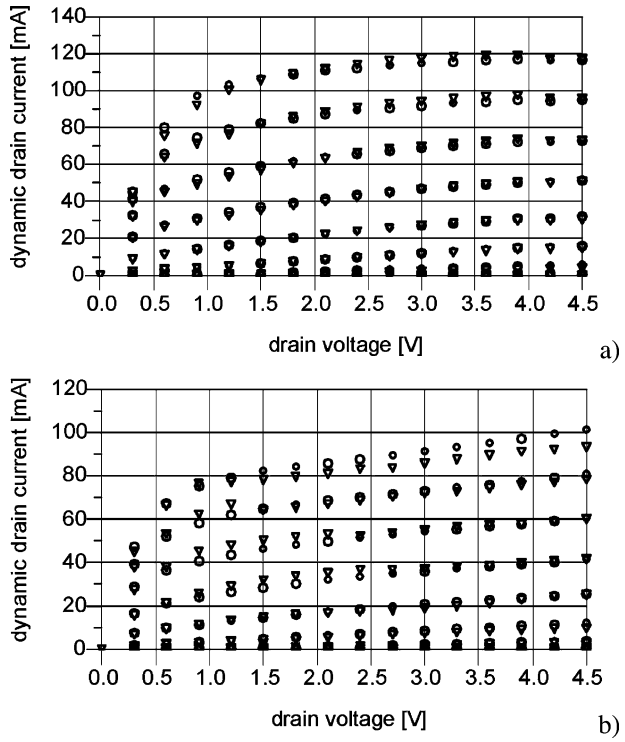

Fig. 9. GaAs 0.25-μm pHEMT dynamic drain current: measurements (circles) versus predictions based on the new model (triangles) for a 50-Ω load condition. In particular, (a) and (b) correspond to dynamic drain current measurements in the same (v_g, v_d) grid of voltages starting from different quiescent conditions [19].

(18), (20), and (21) and the corresponding dynamic measurements obtained under different operating conditions. In particular, large-signal LF I–V data, obtained through the sinusoidal measurement setup [19] recalled in Section I, and SS LF conductances obtained from a conventional vector network analyzer (VNA) were considered here.

B. LF Model Validation

In order to show the SS prediction capabilities of the I–V model, measurements of the pHEMT LF transconductance and output conductance carried out at different bias conditions

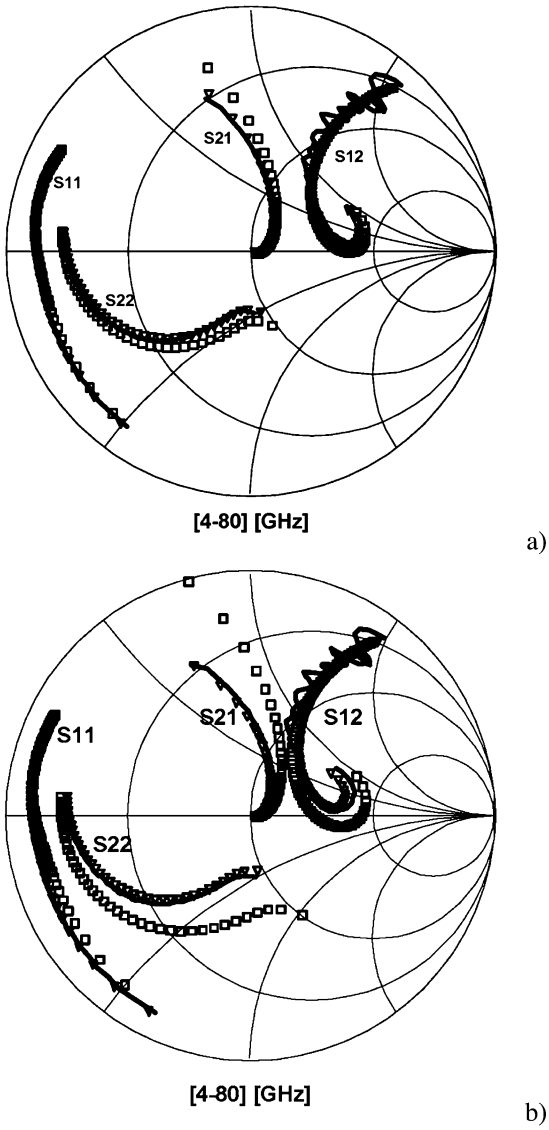

Fig. 10. GaAs 0.25-μm pHEMT S-parameters (opportunely scaled: $S11$, $S12{*}7.4$, $S21/9$, and $S22/1.2$). Measurements (solid lines) are compared to predictions based on the NDC model [2] with embedded the new empirical I–V LF model (triangles) and with the purely static dc I–V characteristics (squares). In particular, (a) and (b) correspond to two different bias conditions, i.e., ($V_{g0} = -0.5$ V, $V_{d0} = 5$ V) and ($V_{g0} = 0.1$ V, $V_{d0} = 3$ V), respectively.

above the cutoff of dispersive phenomena ($f = 2$ MHz) are compared with the model predictions in Figs. 5 and 6. As can be seen, predictions are in excellent agreement with measurements. To provide a wider model validation, using measured data not exploited in the identification phase, pulsed transconductance and output conductance obtained by numerical differentiation of pulsed measurements (bias condition: $V_{g0} = -0.5$ V and $V_{d0} = 5$ V) are compared with the corresponding model predictions in Figs. 7 and 8. Also in this context, a good prediction capability can be observed.

Fig. 9 shows large-signal drain current measurements carried out with the new measurement setup [19] recalled in Section I under 50-Ω loading conditions and coherent current predictions obtained by means of the proposed I–V model. Also in this context, a very good prediction capability of the model can be observed.

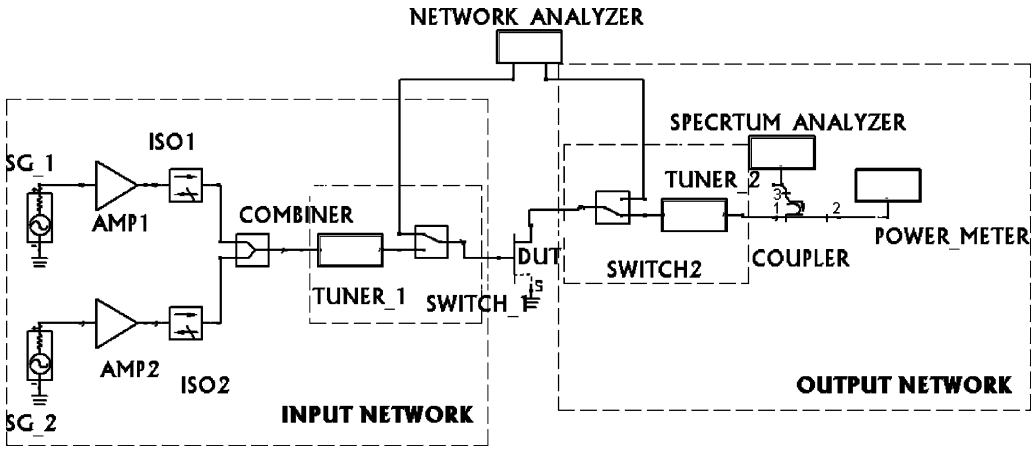

Fig. 11. Experimental intermodulation measurement setup for millimeter-wave applications.

C. High-Frequency Model Validation

The LF model presented in the previous sections was embedded into a nonquasi-static large-signal device model for microwave and millimeter-wave applications, i.e., the NDC model [2]. To this aim, the NDC model was identified on the basis of bias- and frequency-dependent S-parameters carried out by means of a 110-GHz VNA (HP8510XF). A three-delay model structure was used, with $t_M = 1.8$ ps.

To point out the SS microwave frequency prediction accuracy and the improvement due to the new LF I–V model presented, S-parameter measurements carried out in the frequency range 4–80 GHz are shown in Fig. 10 for two different bias conditions. Predictions obtained by means of the NDC model using the new LF dispersive model are reported (triangles) together with the results obtained by using only the purely dc I–V characteristics (squares). In the latter case, limitations to the prediction capabilities are due to the lack of LF dispersion modeling. As can be seen, the prediction performance of the device model, also at microwave frequencies, is strongly affected by the I–V model used to describe the dispersive effects.

In order to evaluate the nonlinear high-frequency prediction accuracy of the model, measurements of the third-order intermodulation product (interferer)-to-carrier ratio (I/C) were carried out at millimeter-wave frequencies on the above-mentioned Triquint pHEMT.

A block diagram of the experimental setup is shown in Fig. 11. Two RF signals are independently generated and amplified before being combined at the input of the DUT. The pHEMT is biased by means of bias tees (omitted in the picture).

The DUT is accessed by means of a half thru standard line, using a probe station. The source and load impedances are settled by means of two passive tuners and measured with an HP8510C VNA.

In order to extend the tuning range of input cell terminations to the low-resistance region, a prematched devices can be used as DUT. In this case, as we will see below, separate cutouts with the input and output prematching networks are needed in order to properly evaluate the source and load device termination.

The input and output networks are connected to the DUT by means of two switches. A 10-dB directional coupler at the output allows the simultaneous measurement of output power by using a power meter and third-order IMD by means of a spectrum analyzer.

In order to evaluate the exact power at the input and output of DUT, and to properly measure the input and output termination, a suitable calibration procedure has been developed. The procedure consists of the following steps.

- Step 1) The power meter is connected directly to the input switch, with SG_2 turned off, evaluating the SG_1 power to set in order to have the desired input power.
- Step 2) The power meter is connected to the output, by connecting together the input and output networks. SG_1 is turned on and setting the power evaluate at Step 1). In this way, output losses can be evaluated.
- Step 3) Input and output are connected by means of a thru line, in order to evaluate losses due to thru and probes. Assuming that the probes have equal losses, the total output losses are evaluated, summing the losses measured in Step 2) with one half of the losses evaluated in Step 3).
- Step 4) SG_1 is set in order to have the desired input power at the half thru reference plane.
- Step 5) The VNA is separately calibrated using a thru reflect line (TRL) calibration, setting the reference planes at half thru line. In order to do that, both RF switches shall be switched.
- Step 6) Switching the input RF switch, the source impedance is measured (i.e., $S(2,2)$ on the VNA), positioning the probes on the thru line. If the DUT is a prematched device, the probes are positioned on the input matching network.

Note that the calibration procedure shall be repeated for every frequency at which the measurements shall be performed.

The third-order IMD measurements are generally performed as a function of output power. Thus, it is important to exactly evaluate the output network losses. Since these losses depend on the load set on the tuner, they should be evaluated for every different chosen load.

The measurement procedure is performed following a number of well-defined steps.

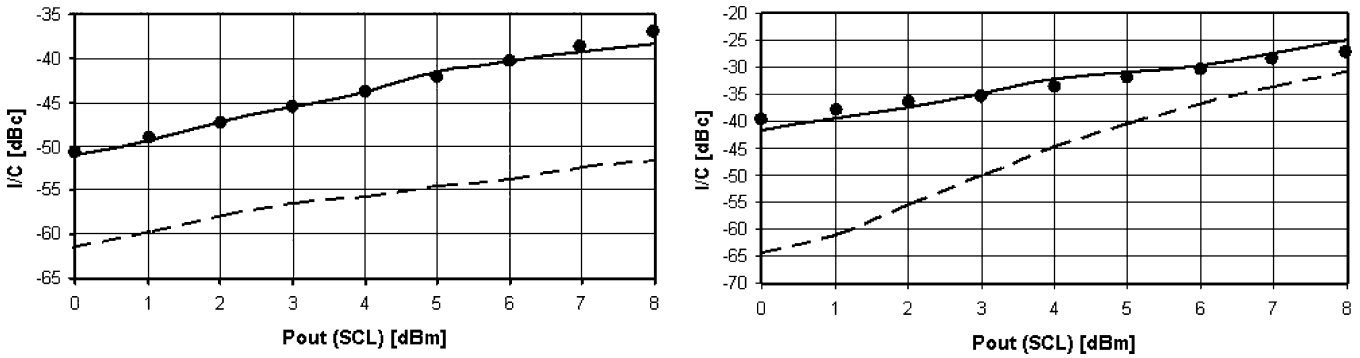

Fig. 12. Third-order I/C versus output power (single carrier level) for the 0.25-μm Triquint GaAs pHEMT at 37 GHz (bias: $I_{d0} = 60$ mA and $V_{d0} = 6.5$ V; load: $Z_L = 14.4 + j * 9.7$ (left) and $Z_L = 48.9 + j * 54.7$ (right); source $Z_S = 49.5 - j * 9.6$). Measurements (circles) are compared to predictions based on the NDC model [2] with the new empirical model embedded (solid line) and with the purely static dc I–V characteristic (dashed line).

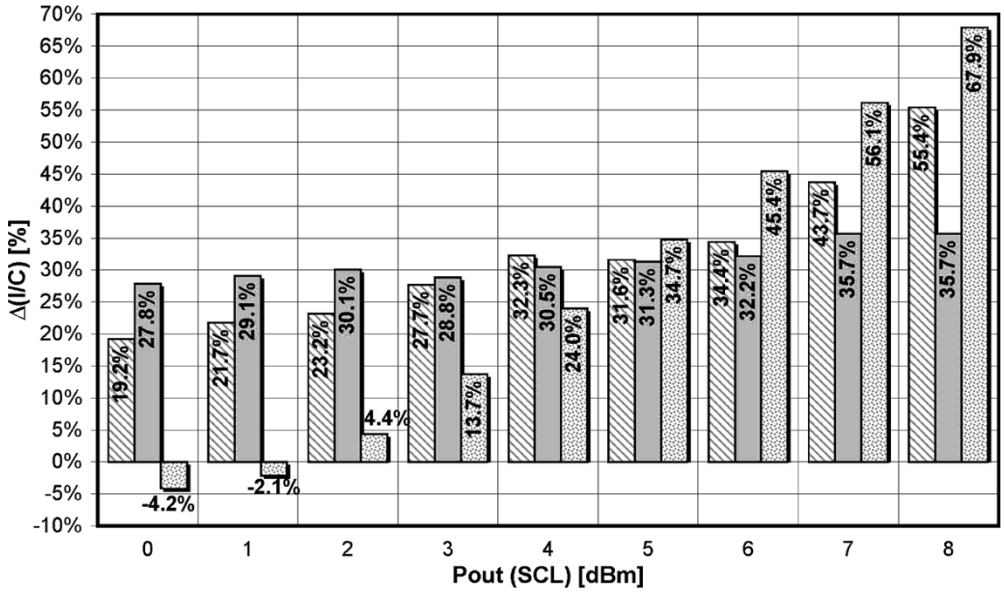

Fig. 13. Variations $\Delta(I/C)_{P_{\text{out}}}^{Z_1,Z_2}$ in the third-order IMD as defined in (22) considering: $Z_1 = 48.9 + j * 54.7$ and $Z_2 = 14.4 + j * 9.7$. Measurements (fulfilled bar) are compared to predictions based on the NDC model [2] with the new empirical model embedded (dashed bar) and with the purely static dc I–V characteristic (dotted bar).

Step 1) The probes are positioned on the thru line. If the DUT is a prematched device, the probes are positioned on the output network.

Step 2) RF switches are set in order to connect port 1 of VNA with the output network.

Step 3) The tuner is set to the desired load, measured with the VNA.

Step 4) The output losses are evaluated setting SG_1 to the power evaluated during the calibration. Since the source and load termination are also known, the pure resistive losses of the output network can be easily evaluated.

Step 5) The probes are positioned on the DUT and the DUT is biased.

Step 6) SG_1 is set in order to have the desired P_{out}. The output power is measured with the power meter.

Step 7) SG_1 is turned off and SG_2 is turned on and set in order to have the same P_{out}.

Step 8) SG_1 is turned on and the third-order IMD measurement is performed by means of the spectrum analyzer.

Measurements of the third-order IMD were carried out at the frequency of 37 GHz (two-tone displacement: 10 MHz; class-A operation: $I_{d0} = 60$ mA and $V_{d0} = 6.5$ V) under different loading conditions. Simulation and measurement results are shown in Fig. 12 as a function of the output power. As can be seen, the model is in very good agreement with measurements.

The ability to predict the microwave PA IMD with different source and load termination values is a very tough validation test for a nonlinear electron device model. In fact, quite often, the device models usually available to the designer do not provide a sufficient level of accuracy in IMD predictions, forcing (e.g., for highly linear PA design) to carry out time-expensive source/load pull characterizations of device samples. In order to test the IMD predictive capability of the proposed model and its ability in providing, by simulation only, a reasonable indication of the near-optimum device termination values, we defined a parameter that takes into account the relative variation of the IMD level by arbitrarily changing the source or the load impedance. More precisely, given two arbitrary loading conditions Z_1 and Z_2 and an output power level P_{out}, we con-

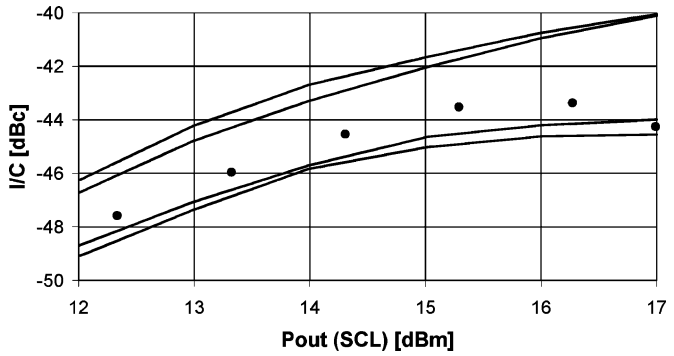

Fig. 14. Measurements (solid lines) of IMD carried out on different PA samples at 38 GHz (bias for the last stage: $I_{d0} = 600$ mA). Predictions based on the new empirical model embedded within the NDC model [2] (circles) are also shown.

sider a parameter $\Delta(I/C)_{P_{\rm out}}^{Z_1,Z_2}$, based on the variation of the third-order IMD, defined as

$$\Delta(I/C)_{P_{\rm out}}^{Z_1,Z_2} = \frac{(I/C)_{P_{\rm out}}^{Z_2} - (I/C)_{P_{\rm out}}^{Z_1}}{(I/C)_{P_{\rm out}}^{Z_1}}. \qquad (22)$$

In Fig. 13, the two loading conditions reported in Fig. 12 have been taken into account; the corresponding $\Delta(I/C)_{P_{\rm out}}^{Z_1,Z_2}$ values are shown for different output power levels. In particular, for each output power condition, measurements (fulfilled bar) are compared to predictions based on the NDC model [2] with the presented LF model (dashed bar) embedded. In the same figure also, the poor prediction capability due to the lack of the LF dispersion modeling, obtained with the purely static I–V characteristics, is shown (dotted bar). Analogous results were obtained for a large number of source and load couples of impedances.

The prediction accuracy of the NDC model has been further tested also by means of a highly linear PA designed and realized by Ericsson with the 0.25-μm Triquint GaAs pHEMT process. The amplifier, namely the Ericsson PA38, works in the 37–40-GHz frequency range and was designed for point-to-point digital radios operating with high spectral efficiency modulation schemes [up to 128 quadrature amplitude modulation (QAM)] [22]. Measurements carried out on the Ericsson PA38 and simulations based on the pHEMT model extracted were compared in [22]. In Fig. 14, measurements of IMD carried out on different PA samples are shown to put in evidence the process dispersion. In the same figure also, the prediction obtained with the model approach proposed is shown.

IV. Conclusion

In this paper, a new current–voltage (I–V) empirical model for the characterization of LF dispersive effects above their cutoff frequencies has been presented. The model formulation has been introduced, then the model identification and validation for a 0.25-μm pHEMT device has been discussed, showing a very good prediction capability under LF small- and large-signal operating conditions.

The empirical model has been embedded in a large-signal device model for microwave and millimeter-wave applications [2]. Intermodulation measurements were carried out at Ka frequencies on a pHEMT device, showing the strong impact of LF dispersive effects on the achievable prediction accuracy also at very high frequencies.

Finally, IMD measurements carried out on different samples of MMIC highly linear PAs have been used to show the possibility of effectively employing this model in the PA design phase as a valuable alternative to expensive load–pull measurements.

References

[1] K. Lu, P. McIntosh, C. M. Snowden, and R. D. Pollard, "Low-frequency dispersion and its influence on the intermodulation performance of AlGaAs/GaAs HBTs," in *IEEE MTT-S Int. Microwave Symp. Dig.*, vol. 3, San Francisco, CA, 1996, pp. 1373–1376.

[2] A. Costantini, R. P. Paganelli, P. A. Traverso, G. Favre, D. Argento, M. Pagani, A. Santarelli, G. Vannini, and F. Filicori, "Accurate prediction of PHEMT intermodulation distortion using the nonlinear discrete convolution model," in *IEEE MTT-S Int. Microwave Symp. Dig.*, vol. 2, Seattle, WA, 2002, pp. 857–860.

[3] P. H. Ladbrooke and S. R. Blight, "Low-field low-frequency dispersion of transconductance in GaAs MESFET's with implications for other rate-dependent anomalies," *IEEE Trans. Electron Devices*, vol. 35, no. 3, pp. 257–267, Mar. 1988.

[4] I. Schmale, F. van Raay, and G. Kompa, "Dispersive table-based large signal FET model validated in analysis of MMIC frequency doubler," in *Proc. 26th Eur. Microwave Conf.*, Prague, Czech Republic, 1996, pp. 260–263.

[5] I. Angelov, L. Bengtsson, and M. Garcia, "Extensions of the Chalmers nonlinear HEMT and MESFET model," *IEEE Trans. Microw. Theory Tech.*, vol. 44, no. 10, pp. 1664–1674, Oct. 1996.

[6] V. I. Cojocaru and T. Brazil, "A scalable general-purpose model for microwave FET's including DC/AC dispersion effects," *IEEE Trans. Microw. Theory Tech.*, vol. 45, no. 12, pp. 2248–2255, Dec. 1997.

[7] K. Jeon, Y. Kwon, and S. Hong, "A frequency dispersion model of GaAs MESFET for large-signal applications," *IEEE Microw. Guided Wave Lett.*, vol. 7, no. 3, pp. 78–80, Mar. 1997.

[8] J. A. Reynoso-Hernandez, L. Escotte, R. Plana, and J. Graffeuil, "Deep level characterization in GaAs FET's by means of the frequency dispersion of the output impedance," *Electron. Lett.*, vol. 31, no. 8, pp. 677–678, Apr. 1995.

[9] D. R. Webster, K. van der Zanden, G. R. Ataei, M. T. Hutabarat, D. Schreurs, and D. G. Haigh, "Large signal frequency dispersion effects in indium phosphide HEMTs," in *IEEE Advances Semiconductor Devices Colloq.*, London, U.K., Jan. 1999 (Ref. 1999/025), pp. 8/1–8/10.

[10] J.-W. Lee and K. J. Webb, "A temperature-dependent nonlinear analytic model for AlGaN–GaN HEMTs on SiC," *IEEE Trans. Microw. Theory Tech.*, vol. 52, no. 1, pp. 2–9, Jan. 2004.

[11] M. Fernández-Barciela, P. J. Tasker, Y. Campos-Roca, M. Demmler, H. Massler, E. Sánchez, C. Currás-Francos, and M. Schlechtweg, "A simplified broad-band large-signal non quasi-static table-based FET model," *IEEE Trans. Microw. Theory Tech.*, vol. 48, no. 3, pp. 395–405, Mar. 2000.

[12] J. M. Golio, M. G. Miller, G. N. Maracas, and D. A. Johnson, "Frequency-dependent electrical characteristics of GaAs MESFET's," *IEEE Trans. Electron Devices*, vol. 37, no. 5, pp. 1217–1227, May 1990.

[13] N. Scheinberg, R. Bayruns, and R. Goyal, "A low frequency GaAs MESFET circuit model," *IEEE J. Solid-State Circuits*, vol. 23, no. 2, pp. 605–608, Apr. 1988.

[14] T. Roh, Y. Kim, Y. Suh, W. Park, and B. Kim, "A simple and accurate MESFET channel-current model including bias-dependent dispersion and thermal phenomena," *IEEE Trans. Microw. Theory Tech.*, vol. 45, no. 8, pp. 1252–1255, Aug. 1997.

[15] J. Rodriguez-Tellez, T. Fernandez, A. Mediavilla, and A. Tazon, "Characterization of thermal and frequency-dispersion effects in GaAs MESFET devices," *IEEE Trans. Microw. Theory Tech.*, vol. 49, no. 7, pp. 1352–1355, Jul. 2001.

[16] A. E. Parker and D. E. Root, "Pulse measurements quantify dispersion in pHEMT's," in *Proc. URSI/IEEE Electronics Signals Systems Symp.*, Pisa, Italy, Oct. 1998, pp. 444–449.

[17] J. B. Scott, J. G. Rathmell, A. E. Parker, and M. Sayed, "Pulsed device measurements and applications," *IEEE Trans. Microw. Theory Tech.*, vol. 44, no. 12, pp. 2718–2723, Dec. 1996.

[18] J. P. Teyssier, P. Bouysse, Z. Ouarch, D. Barataud, T. Peyretaillade, and R. Quere, "40 GHz/150-ns versatile pulsed measurement system for microwave transistor isothermal characterization," *IEEE Trans. Microw. Theory Tech.*, vol. 46, no. 12, pp. 2043–2052, Dec. 1998.

[19] A. Raffo, A. Santarelli, P. A. Traverso, G. Vannini, and F. Filicori, "On-wafer I/V measurement setup for the characterization of low-frequency dispersion in electron devices," in *IEEE 63rd Automatic RF Techniques Group Microwave Measurements Conf. Dig.*, Fort Worth, TX, 2004, pp. 21–28.

[20] A. Santarelli, G. Vannini, F. Filicori, and P. Rinaldi, "Backgating model including self-heating for low-frequency dispersive effects in III–V FETs," *Electron. Lett.*, vol. 34, no. 20, pp. 1974–1976, Oct. 1998.

[21] F. Filicori, G. Vannini, A. Santarelli, A. M. Sanchez, A. Tazon, and Y. Newport, "Empirical modeling of low-frequency dispersive effects due to traps and thermal phenomena in III–V FET's," *IEEE Trans. Microw. Theory Tech.*, vol. 43, no. 12, pp. 2972–2981, Dec. 1995.

[22] A. Raffo, A. Santarelli, P. A. Traverso, M. Pagani, F. Palomba, F. Scappaviva, G. Vannini, and F. Filicori, "Improvement of PHEMT intermodulation prediction through the accurate modeling of low-frequency dispersion effects," in *IEEE MTT-S Int. Microwave Symp. Dig*, Long Beach, CA, 2005. [CD ROM].

[23] C. Fiegna, F. Filicori, G. Vannini, and F. Venturi, "Modeling the effects of traps on the I–V characteristics of GaAs MESFETs," in *Int. Electron Devices Meeting*, Washington, DC, 1995, pp. 773–776.

Antonio Raffo (S'04) was born in Taranto, Italy, in 1976. He received the Laurea degree (with honors) in electronic engineering from the University of Ferrara, Ferrara, Italy, in 2002, and is currently working toward the Ph.D. degree at the University of Ferrara.

Since 2002, he has been with the Electronic Department, University of Ferrara. He also collaborates with CoRiTel Research Consortium, Morean (Rome), Italy. His research activity is mainly oriented to nonlinear electron device modeling and circuit design techniques for nonlinear microwave and millimeter-wave applications.

Dr. Raffo was the recipient of the Student Paper Prize presented at the 2005 European Gallium Arsenide and Other Compound Semiconductors Application Symposium.

Alberto Santarelli (M'96) received the Laurea degree in electronic engineering and Ph.D. degree in electronics and computer science from the University of Bologna, Bologna, Italy, in 1991 and 1996, respectively.

From 1996 to 2001, he was a Research Assistant with the Research Center for Computer Science and Communication Systems, Italian National Research Council (IEIIT-CNR), Bologna, Italy. Since 2001, he has been with the Department of Electronics, Computer Science and Systems (DEIS), University of Bologna, Bologna, Italy, where he is currently an Associate Professor. During his academic career, he has been a Lecturer of applied electronics, industrial electronics, and electronics for telecommunications. His main research interests are electron device nonlinear modeling and circuit design for nonlinear microwave applications.

Pier Andrea Traverso (M'03) was born in Modena, Italy, in 1969. He received the M.S. degree in electronic engineering and Ph.D. degree in electronic and computer science engineering from the University of Bologna, Bologna, Italy, in 1996 and 2000, respectively.

He is currently a Research Associate with the Department of Electronics, Computer Science and Systems, University of Bologna. His main research activity is in the areas of nonlinear dynamic system characterization and modeling, microwave and millimeter-wave device characterization and modeling, and sampling instrumentation.

Dr. Traverso is a member of the Italian Association on Electrical and Electronic Measurements.

Giorgio Vannini (S'87–M'92) received the Laurea degree in electronic engineering and Ph.D. degree in electronic and computer science engineering from the University of Bologna, Bologna, Italy, in 1986 and 1992, respectively.

In 1992, he joined the Department of Electronics, University of Bologna, as a Research Associate. Since 1994, he has been also with the Institute for Electronics, Telecommunication and Information Engineering, National Research Council. Since November 1998, he has been an Associate Professor with the Faculty of Engineering, Department of Engineering, University of Ferrara, Ferrara, Italy where he is currently a Full Professor of electronics. During his academic career, he has been a Teacher of applied electronics, electronics for communications, and industrial electronics. He has coauthored over 120 papers published in international journals and conferences His research activity is mainly devoted to electron device modeling, computer-aided design (CAD) techniques for MMICs, and nonlinear circuit analysis and design.

Prof. Vannini is a member of the Italian Federation of Electrical and Electronic Engineering (AEIT) and the Gallium Arsenide Application Symposium Association (GAAS). He was the recipient of the Best Paper Prize presented at the 25th European Microwave Conference.

Francesco Palomba was born in Naples, Italy, in 1971. He received the M.S. degree in solid-state physics and Ph.D. degree in applied physics from the University of Naples "Federico II," Naples, Italy, in 1996 and 1999, respectively.

In 2000, he joined the Ericsson Laboratory Italy S.p.A., Vimodrone (MI), Italy, where he is currently involved with GaAs MMIC design for digital radio applications. He has been involved with research in the field of RF and microwave superconductivity. His current research activities are related to high linearity PAs for Ku, K, and Ka frequency bands.

Francesco Scappaviva was born in Lecce, Italy, in 1978. He received the Laurea degree in electronic engineering from the University of Bologna, Bologna, Italy, in 2004.

In 2004, he joined Microwave Electronics for Communications S.r.l. (MEC), Bologna, Italy, where he is currently an RF Research Engineer. His research is mainly oriented to microwave integrated circuit design. His main research interests are in the field of RF PAs for space applications.

Maurizio Pagani was born in Borgomanero, Italy, in 1963. He received the Laurea degree in electronic engineering from the Politecnico di Torino, Turin, Italy, in 1988.

In 1988, he joined Telettra S.p.A., Vimercate, Italy, where he was a Researcher with the GaAs Laboratory involved in characterization and modeling of microwave devices and MMICs. From 1992 to 1998, he was responsible for the Microwave Integrated Circuit Design Group, Alcatel Italia. In 1998, he joined the Microwave Product Design Centre, Ericsson Laboratory Italy, Milan, Italy, where he is currently the Manager of the MMIC Design Unit. He also collaborates with the CoRiTel Research Consortium and is also a Contract Professor of microwave integrated circuits with the University of Florence, Florence, Italy. He has authored or coauthored over 20 papers in international scientific journals and conferences. His main research interests are in the field of low-cost solutions of integrated circuit design, highly linear PAs, and linearization techniques for microwave radio applications. In these areas, he has been involved in several research activities.

Fabio Filicori was born in Imola, Italy, in 1949. He received the Electronic Engineering degree from the University of Bologna, Bologna, Italy, in 1974.

He is currently a Full Professor of applied electronics with the University of Bologna. His current research interests are in the areas of nonlinear circuit analysis and design, electronic devices modeling, digital measurement instruments, and power electronics.